Hydrogenase Models

DOI: 10.1002/anie.201006244

A Model of the [FeFe] Hydrogenase Active Site with a Biologically Relevant Azadithiolate Bridge: A Spectroscopic and Theoretical Investigation**

Özlen F. Erdem, Lennart Schwartz, Matthias Stein, Alexey Silakov, Sandeep Kaur-Ghumaan, Ping Huang, Sascha Ott,* Edward J. Reijerse, and Wolfgang Lubitz**

The active site of [FeFe] hydrogenase, the so-called H-cluster, is composed of a [4Fe4S] cubane that is connected to a [2Fe2S] subcluster by a cysteine residue.[1] These hydrogenases are predominantly involved in hydrogen evolution, which makes them an attractive starting point for the development of biotechnological and bioinspired hydrogen production systems.[2]

The two iron centers of the binuclear subcluster in the [FeFe] hydrogenase are coordinated by unusual non-protein CN^- and CO ligands that stabilize their low spin and oxidation state (H_{ox} and H_{ox}-CO in Scheme 1).[3,4] The iron center distal to the cubane in the H_{ox} state (Fe_d) has an open coordination site where hydrogen or CO as inhibitor can bind. The central atom in the dithiolate bridging ligand (depicted as NH in Scheme 1) could equally well be modeled as carbon, oxygen, or nitrogen in X-ray crystallography.[1b] In view of the catalytic mechanism, a nitrogen atom,[1c] and to some extent also an oxygen atom,[1f] could function as an effective proton relay,[1b,g] helping to split H_2, and thus shuttling protons between the binuclear subcluster and the nearby cysteine residue that is believed to be part of the proton channel.[5] Recently, a combined electron paramagnetic resonance (EPR) spectroscopic and density functional theory (DFT) study on the [FeFe] hydrogenase active site of *Desulfovibrio desulfuricans*[6] provided strong evidence for a nitrogen atom in the bridging dithiolate. This assignment was based on the obtained quadrupole couplings of three distinct types of nitrogen atom (amine, cyanide, and lysine side chain) detected in the hyperfine sublevel correlation (HYSCORE) spectrum.[6]

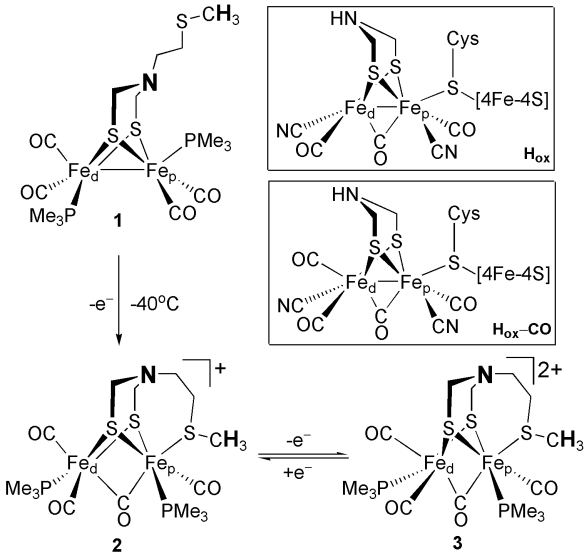

Scheme 1. Structural rearrangement of complex **1** upon (electro)chemical oxidation at −40 °C; sites of isotope labeling are highlighted in bold face. Compound **1**: Fe^IFe^I state, **2**: $Fe^{II}Fe^I$ state, **3**: $Fe^{II}Fe^{II}$ state. Inset: H-cluster of the [FeFe] hydrogenase in the H_{ox} and the CO-inhibited state (H_{ox}-CO); both have a $Fe_d^{II}Fe_p^I$ configuration.

Further indications for the presence of nitrogen in the dithiolate ligand (azadithiolate, adt) come from bioinorganic model systems.[7] It is well-established that N-protonation leads to species that feature greatly decreased reduction potentials compared to their non-protonated counterparts with all-carbon linkers.[8] Furthermore, the adt nitrogen can act as a proton relay in model compounds by shuffling protons to the open coordination site of suitable model complexes to afford terminal hydride species.[9]

To further verify the nature of the central atom in the dithiolate bridge in the H-cluster of the [FeFe] hydrogenase, we studied a mixed-valence $Fe^{II}Fe^I$ model complex that features only one nitrogen atom in the molecule. For this purpose, the "native" CN ligands were replaced by electronically analogous trimethylphosphine ligands. Herein we present the first detailed analysis of the electronic structure of such a mixed-valence biomimetic complex and compare the

[*] Dr. Ö. F. Erdem, Dr. A. Silakov, Dr. E. J. Reijerse, Prof. Dr. W. Lubitz
Max-Planck-Institut für Bioanorganische Chemie
Stiftstrasse 34-36, 45470 Mülheim an der Ruhr (Germany)
Fax: (+49) 208-306-3955
E-mail: erdem@mpi-muelheim.mpg.de
lubitz@mpi-muelheim.mpg.de
Dr. L. Schwartz, Dr. S. Kaur-Ghumaan, Dr. P. Huang, Dr. S. Ott
Department of Photochemistry and Molecular Science
Uppsala University, Box 523, 75120 Uppsala (Sweden)
E-mail: sascha.ott@fotomol.uu.se
Dr. M. Stein
Max-Planck-Institut für Dynamik komplexer technischer Systeme
Sandtorstrasse 1, 39106 Magdeburg (Germany)

[**] Gudrun Klihm is gratefully acknowledged for her technical support in the EPR experiments. Financial support from the Max Planck Society, the Swedish Research Council (S.O.), the Wenner Gren Foundation (S.K.-G.), the Swedish Energy Agency, the Knut and Alice Wallenberg Foundation, the Klaus Tschira Foundation (M.S.), and the EU (FP7 Energy 212508 "SOLAR-H2") is gratefully acknowledged.

Supporting information for this article is available on the WWW under http://dx.doi.org/10.1002/anie.201006244.

results with those observed for the native system. As illustrated in Scheme 1, the mixed-valence species **2** is a close structural mimic of H_{ox}-CO and is available from complex **1** upon oxidation below −30 °C. Complex **1**, in turn, was prepared from 2-(methylthio)ethylamine, $[Fe_2S_2(CO)_6]$, and formaldehyde, as described earlier.[10] ^{15}N-labeled (**1**[^{15}N]) and CD_3-labeled (**1**[S−CD_3]) complexes were prepared from the corresponding isotope labeled precursors in the same way (see the Supporting Information).

Electrochemical investigation by cyclic voltammetry (CV) reveals that **1** is irreversibly oxidized in a two-electron process at room temperature (Figure 1 a). Lowering the temperature below −30 °C has a dramatic effect on the CV: The irreversible wave decreases in amplitude to a level that corresponds to a one-electron process ($Fe^IFe^I \rightarrow Fe^IFe^{II}$). At the same time, a new second, reversible wave emerges at slightly more positive potential than the first. This behavior is consistent with an irreversible chemical process that occurs upon the first oxidation to form a species which can be reversibly oxidized in a second process, namely $Fe^IFe^{II} \rightleftarrows Fe^{II}Fe^{II}$. Chemical oxidation of **1** by ferrocenium hexafluorophosphate ($FcPF_6$) at −30 °C occurs in an analogous way and was followed by in situ FTIR spectroscopy (Figure 1 b). Addition of one equivalent of $FcPF_6$ shifts all absorptions in the ν_{CO} region towards higher energy as a result of oxidation, and thus decreases backbonding into the CO-based π* orbitals. At the same time, a new absorption band emerges at 1770 cm^{-1}, which is diagnostic for a μ-CO ligand bridging the two Fe centers.

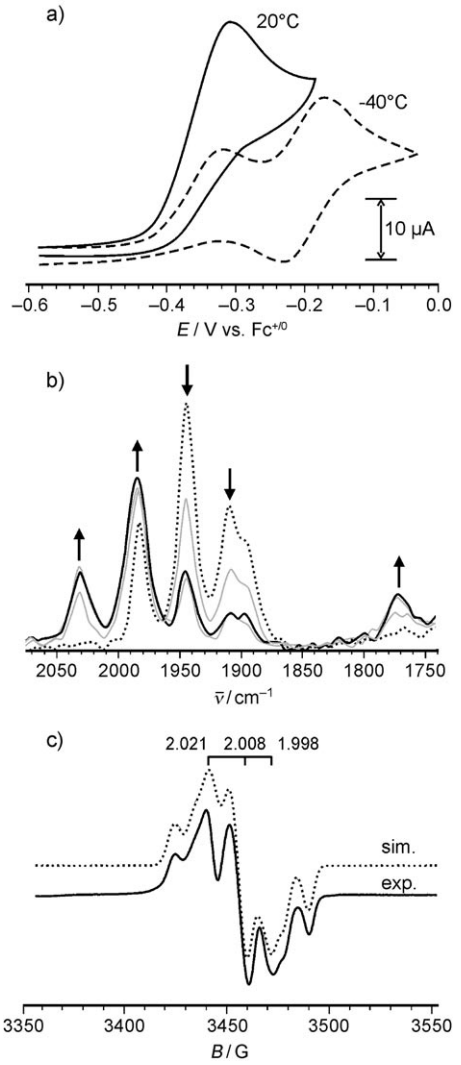

Figure 1. a) Cyclic voltammetry (oxidation scan) of 1 mM solutions of **1** in CH_3CN at 20 °C (——) and −40 °C (•••••). b) In situ FTIR spectra recorded every 5 s after addition of $FcPF_6$ (1 equiv) to solutions of **1** in CH_3CN at −40 °C. ••••• Starting spectrum, —— final spectrum; c) CW EPR spectrum of **2** (in 2-MeTHF/CH_2Cl_2) recorded at X-band at 30 K. —— experiment, ••••• simulation (principal *g* values, *g*(*x*,*y*,*z*): (2.021, 2.008, 1.998); *g* strain: 0.0038, 0.0025, 0.0043; linewidth: 0.6 mT).

The electrochemical and IR-spectroscopic behavior of **2** resembles that of a related $Fe^{II}Fe^I$ mixed-valence species described by Pickett and co-workers, [2Fe3S] dicyanide (**4**), that features CN^- instead of PMe_3 ligands, but lacks the adt nitrogen atom.[11] Although the IR spectra of the two species are very similar in shape, the structural differences between the two complexes lead to a shift of the vibrational frequencies in **2** to lower wavenumbers. In analogy to **4** and as shown by our studies (see below), it is clear that the first oxidation of **1** to **2** is stabilized by the thioether substituent that coordinates to Fe_p upon oxidation. The second oxidation to form **3** is a simple electron loss that does not cause any further structural changes.

A single-crystal X-ray structure determination of **1** (see the Supporting Information) reveals an apical/basal arrangement of the PMe_3 ligands. DFT calculations of **1** (see the Supporting Information) closely reproduce its X-ray structure. The calculations also suggest a structural model for the oxidized Fe^IFe^{II} complex **2** in which the oxidation is accompanied by formation of an additional iron–thioether bond with a bond length of 2.50 Å, creation of a μ-bridging CO, and reorientation of the PMe_3 ligands. The calculated IR spectra of **1** and **2** are in agreement with the experimental FTIR data presented in Figure 1 b (see also the Supporting Information). For **2**, a *trans* basal/basal conformation of the PMe_3 ligands is lowest in energy. A *cis* basal/basal or basal/apical PMe_3 orientation is higher in energy by 3 and 5 kcal mol^{-1}, respectively.

The molecular integrity of the mixed-valence complex **2** could be further confirmed by CW-EPR spectroscopy. The X-band CW-EPR spectrum at 30 K of **2** prepared in 2-methyltetrahydrofuran (2-MeTHF)/CH_2Cl_2 is presented in Figure 1 c. The corresponding simulations are performed assuming a single $S = 1/2$ paramagnetic species with hyperfine couplings (HFCs) to two distinct ^{31}P nuclei. The CW EPR spectrum can be accurately simulated using a rhombic *g* tensor, where $g_x > g_y > g_z$: $g(x,y,z) = (2.021,\ 2.008,\ 1.998)$; with HFC values of $A_1(^{31}P)$ $(x,y,z) = (34,\ 27,\ 28)$ MHz and $A_2(^{31}P)$ $(x,y,z) = (50,\ 26,\ 47)$ MHz. DFT calculations suggest that a rhombic *g* tensor is obtained for both basal/basal and apical/basal orientation of the PMe_3 ligands. However, an apical/basal orientation of these ligands would lead to an unusually large isotropic ^{31}P hyperfine interaction for the apical phosphorus atom (see the Supporting Information). Such a situation can be ruled out for **2**. The fact that the HFC

values for the two ^{31}P nuclei are similar points to a delocalization of the unpaired electron spin over both iron centers in the complex. The best agreement between experimental and calculated ^{31}P HFC values is obtained for a spin-delocalized *trans* basal/basal arrangement of the PMe_3 ligands (see the Supporting Information). Broken-symmetry DFT calculations also result in a spin-delocalized state. The larger isotropic HFC is obtained for the proximal ^{31}P nucleus (spin density at the proximal Fe is 0.54, at the distal Fe is 0.23; see Figure 2 and the Supporting Information).[12,13]

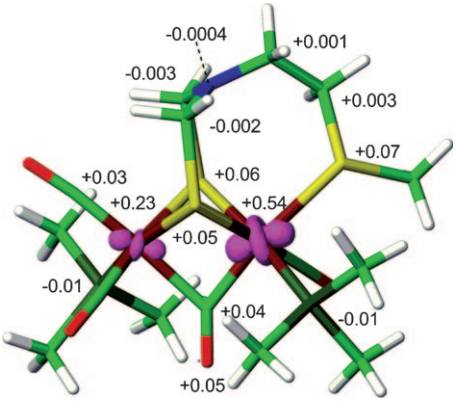

Figure 2. Calculated unpaired spin-density distribution in **2**, together with the Mulliken atomic spin populations.

The *g* values are less anisotropic than those obtained for the native hydrogenase H_{ox}-CO inhibited state, which are $g(x,y,z) = (2.065, 2.007, 2.001)$.[6] In comparison, the CW EPR spectrum of the cyanide-containing complex **4**[11a] revealed *g* values of $g(x,y,z) = (2.017, 2.006, 1.988)$ for which the anisotropy is close to that of **2**. A model complex of H_{ox} investigated by Darensbourg and co-workers,[14] $[Fe_2(dmpdt)(CO)_4(PMe_3)_2]^+$ (dmpdt = μ-2,2-dimethyl-1,3-propanedithiolate), showed a *g* tensor of $g(x,y,z) = (2.086, 2.025, 2.007)$ and a ^{31}P HFC tensor of $A(x,y,z) = (27, 25, 25)$ MHz. The CW EPR spectral data was interpreted as suggesting a localization of the spin density on one of the irons. For the H-cluster in the H_{ox} state, however, a delocalization over both iron atoms was found while the data for the H_{ox}-CO state pointed to a localization on the proximal iron.[4] It is tempting to assume that these differences are related to the presence of the [4Fe4S] cubane subcluster in the H-cluster; this unit is absent in the model complexes (see below).

The coordination of the S–CH_3 thioether group to Fe_p in **2** was further investigated by a spectroscopic comparison with **2**[S–CD_3], which contains a deuterated (S–CD_3) group. The relatively weak hyperfine couplings of the methyl protons are not resolved in the CW EPR spectrum. We have therefore performed electron nuclear double-resonance (ENDOR)[15a] experiments to improve the spectral resolution.

In Figure 3, the Q-band ^1H Davies ENDOR results for **2**[S–CD_3] and **2**[S–CH_3] are compared. The difference spectrum (Figure 3c), containing the features attributed only to the S–CH_3 protons, is simulated using HFC values

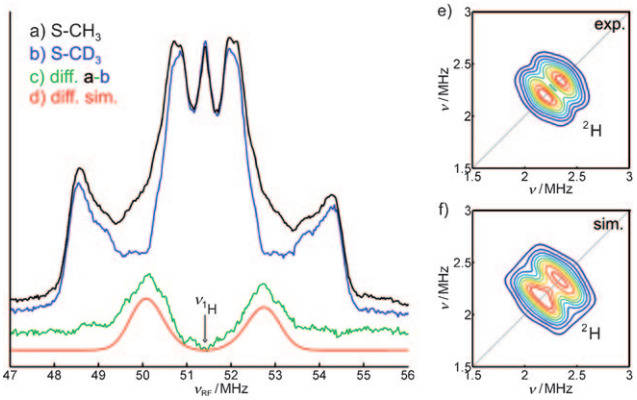

Figure 3. Q-band Davies ENDOR spectra of a) **2**, b) **2**[S–CD_3] (in 2-MeTHF/CH_2Cl_2), c) difference spectrum, and d) the corresponding simulation for the difference spectrum, recorded at a field position corresponding to g_y, $T = 30$ K. e) X-band HYSCORE spectrum of **2**[S–CD_3] recorded with $\tau = 212$ ns at $T = 30$ K, field position: g_y (see the Supporting Information for details). f) Corresponding simulation for (e).

of $A(x,y,z) = (2.6, -2.6, -3.6)$ MHz, $A_{iso}(^1H) = -1.2$ MHz. Furthermore, a ^2H HYSCORE experiment was performed on **2**[S–CD_3] (Figure 3e). The simulation (Figure 3f) was performed by means of the spin Hamiltonian approach.[15a,b,c] The parameters used for simulation are as follows: $A_{iso}(^2H) = -0.2$ MHz, $K = 0.06$ MHz, $\eta = 0.01$, where $K = e^2qQ/4h$ is the quadrupole coupling and η is the asymmetry parameter.[16] The deuterium HFC, $A_{iso}(^2H)$, is consistent with the 6.514-fold scaling factor in the Larmor frequency for ^2H compared to ^1H. The unpaired spin density at the S–CH_3 group is small but significant and can only be explained by the proposed structural rearrangement for the metastable Fe^IFe^{II} state where the S–CH_3 group directly coordinates to the proximal iron atom (Scheme 1). The DFT predictions for the HFC and NQC values for the S–CH_3 and S–CD_3 groups are in good agreement with the measured values, and provide additional support for the spectral assignment (see the Supporting Information and Table 1).

Figure 4 shows the X-band matched-HYSCORE[15a] spectra for **2**[^{14}N] and the ^{15}N-labeled complex **2**[^{15}N]. The Larmor frequency of ^{14}N at the X band is 1.062 MHz. It is known that for systems with strong quadrupole coupling and weak anisotropy of the HFC, the corresponding single quantum

Table 1: Comparison of experimental and DFT calculated HFC and NQC principal values [MHz] for the basal/basal *trans* isomer of **2** (PMe_3, adt-*N*, S–CD_3) and for H_{ox}.[6]

	2 (DFT)	**2** (exp.)	H_{ox}[6]
$A_{iso1}(^{31}P)$	−37	41 ± 2	–
$A_{iso2}(^{31}P)$	−28	30 ± 2	–
$A_{iso}(^{14}N)$	1.0	0.6 ± 0.2	1.43
K	1.32	1.28 ± 0.01	1.23
η	0.03	0.11 ± 0.05	0.13
$A_{iso}(^2H)$	−0.3	−0.2 ± 0.1	–
K	0.05	0.06 ± 0.05	–
η	0.03	0.01 ± 0.05	–

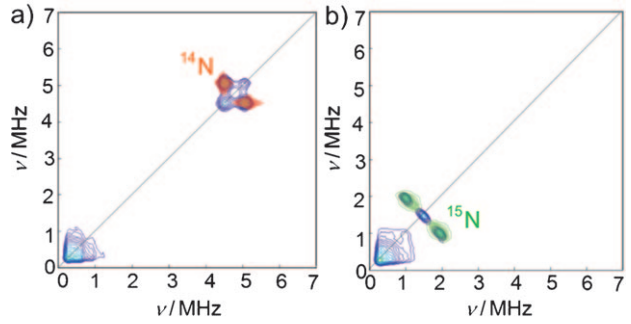

Figure 4. X-band matched-HYSCORE[15a] spectra for a) **2**[^{14}N], b) **2**[^{15}N] (in 2-MeTHF/CH_2Cl_2) recorded with $t_{matching} = 72$ ns, $\tau = 128$ ns at $g_y = 2.008$ (as indicated in Figure 1c), at 30 K. Corresponding simulations are indicated with orange lines for **2**[^{14}N] and with green lines for **2**[^{15}N] (for details, see Table 1 and the Supporting Information).

transitions may be invisible in HYSCORE.[15a,c] The two ^{14}N correlation peaks (Figure 4a) are centered at about 4.8 MHz. Their positions are typical for the ^{14}N ($I = 1$) double quantum transitions of a weakly coupled nitrogen nucleus with relatively strong quadrupole interaction. For the matched-HYSCORE spectra, the features can be simulated using principal HFC values of $A(^{14}N)(x,y,z) = (0.3, 0.8, 0.7)$ MHz, and quadrupole parameters of $K = 1.28$ MHz and $\eta = 0.11$ (see Table 1). In the corresponding matched HYSCORE spectrum of **2**[^{15}N] (Figure 4b), the correlation features at about 4.8 MHz are absent, and instead resonances are found at 1.489 MHz, which is the Larmor frequency of ^{15}N. These peaks are due to the basic spin transitions for an $I = 1/2$ nucleus, and can be simulated using the HFC tensor found for **2**[^{14}N] scaled with the 1.402-fold scaling factor in the Larmor frequency for ^{15}N compared to ^{14}N.

The obtained coupling parameters are summarized in Table 1 together with those found for the H-cluster in the H_{ox} state.[6] The ^{14}N HFC and NQC values that were calculated by DFT are in good agreement with the simulated values. The asymmetry parameter η is, however, slightly underestimated in the DFT calculations (see for example Ref. [17a,b]). In principle, the NQC values are sensitive to the protonation state of the amino group. Protonation that would lead to a secondary ammonium group ($-NH_2^+-$) can however be ruled out owing to its small K value. In quantum refinement investigations on [FeFe] hydrogenase active site models, this possibility was however still discussed.[17c] An explicit hydrogen bond (coordination of an external water molecule to the amine nitrogen) has only a small influence on the ^{14}N HFC and NQC values (see the Supporting Information for details).

In general, the DFT calculations reveal that the unpaired spin distribution of **2** clearly differs from that of the H-cluster in the H_{ox}-CO state. Whereas in **2** both iron atoms carry unpaired spin density (also concluded from the similar ^{31}P HFC values), the spin density for the H_{ox}-CO state is shifted towards the proximal iron in the binuclear subcluster.[4] For the native system, owing to the strong exchange interaction between the cubane and binuclear subcluster in the H_{ox}-CO state, most of the spin density is shifted towards the [4Fe4S] cubane and very little is left on the binuclear $[2Fe]_H$ subcluster. Therefore, the ^{14}N couplings of the CN ligands and the bridging azadithiolate are too small to be detectable. For complex **2**, on the other hand, all spin density resides on the binuclear cluster and sufficient spin density appears to be present at the bridging adt N atom for the ^{14}N coupling to be observable by HYSCORE spectroscopy. In fact, the unpaired spin distribution of **2** bears more similarity with that of the native H_{ox} state, in which the weakening of the exchange interaction between the cubane and the [2Fe] cluster allows more effective spin density to be present at the $[2Fe]_H$ subcluster and thus to detect ^{14}N signals from the amino ligand.[6] Indeed, the ^{14}N nuclear quadrupole interaction for **2** and for H_{ox} (Table 1) are very similar. Their quadrupole parameter K is characteristic[16b] for a weakly H-bonded amino nitrogen atom.

In summary, our investigations show that upon oxidation of **1** to the mixed-valence state **2**:

a) one terminal CO ligand moves into the bridging position;
b) the pendant thioether group bends over and coordinates the "proximal" iron atom;
c) the ligand sphere rearranges and one of the PMe_3 ligands moves into a basal position, probably leading to a *trans* basal/basal configuration of the two PMe_3 groups; and
d) the HFC components obtained for the amino nitrogen in the azadithiolate bridge of **2** are quite similar to those found for the H_{ox} state, showing that the spin density indeed extents onto the amino group of the bridging adt ligand. The measured NQC of the respective ^{14}N in **2** is also similar to that observed in the H-cluster. Its value is characteristic for a weakly hydrogen bonded amino group.[16b] These similarities provide convincing evidence for the presence of a nitrogen atom in the dithiolate bridge of the active site of native [FeFe] hydrogenases. This finding is of great importance for understanding the mechanism of dihydrogen conversion/production, and probably also for the very high activity of this enzyme.[8,9]

Received: October 5, 2010
Published online: January 5, 2011

Keywords: density functional calculations · ENDOR spectroscopy · enzyme models · EPR spectroscopy · hydrogenases

[1] a) Y. Nicolet, B. J. Lemon, J. C. Fontecilla-Camps, J. W. Peters, *Trends Biochem. Sci.* **2000**, *25*, 138–143; b) J. C. Fontecilla-Camps, P. Amara, C. Cavazza, Y. Nicolet, A. Volbeda, *Nature* **2009**, *460*, 814–822; c) Y. Nicolet, A. L. de Lacey, X. Vernéde, V. M. Fernandez, E. C. Hatchikian, J. C. Fontecilla-Camps, *J. Am. Chem. Soc.* **2001**, *123*, 1596–1601; d) Y. Nicolet, C. Piras, P. Legrand, C. E. Hatchikian, J. C. Fontecilla-Camps, *Structure With Folding & Design* **1999**, *7*, 13–23; e) J. W. Peters, W. N. Lanzilotta, B. J. Lemon, L. C. Seefeldt, *Science* **1998**, *282*, 1853–1858; f) A. S. Pandey, T. V. Harris, L. J. Giles, J. W. Peters, R. K. Szilagyi, *J. Am. Chem. Soc.* **2008**, *130*, 4533–4540; g) H.-J. Fan, M. B. Hall, *J. Am. Chem. Soc.* **2001**, *123*, 3828–3829.

[2] a) R. Cammack, M. Frey, R. Robson, *Hydrogen as a Fuel. Learning from Nature*, Taylor & Francis, London, **2001**;

b) D. A. J. Rand and R. M. Dell, *Hydrogen Energy. Challenges and Prospects*, RSC, Cambridge, **2008**.
[3] W. Roseboom, A. L. De Lacey, V. M. Fernandez, E. C. Hatchikian, S. P. J. Albracht, *J. Biol. Inorg. Chem.* **2006**, *11*, 102 – 118.
[4] A. Silakov, E. J. Reijerse, S. P. J. Albracht, E. C. Hatchikian, W. Lubitz, *J. Am. Chem. Soc.* **2007**, *129*, 11447 – 11458.
[5] J. C. Fontecilla-Camps, A. Volbeda, C. Cavazza, Y. Nicolet, *Chem. Rev.* **2007**, *107*, 4273 – 4303.
[6] A. Silakov, B. Wenk, E. Reijerse, W. Lubitz, *Phys. Chem. Chem. Phys.* **2009**, *11*, 6592 – 6599.
[7] For reviews see: a) C. Tard, C. J. Pickett, *Chem. Rev.* **2009**, *109*, 2245 – 2274; b) J. F. Capon, F. Gloaguen, F. Y. Pétillon, P. Schollhammer, J. Talarmin, *Coord. Chem. Rev.* **2009**, *253*, 1476 – 1494; c) G. A. N. Felton, C. A. Mebi, B. J. Petro, A. K. Vannucci, D. H. Evans, R. S. Glass, D. L. Lichtenberger, *J. Organomet. Chem.* **2009**, *694*, 2681 – 2699; d) D. M. Heinekey, *J. Organomet. Chem.* **2009**, *694*, 2671 – 2680; e) F. Gloaguen, T. B. Rauchfuss, *Chem. Soc. Rev.* **2009**, *38*, 100 – 108; f) R. Lomoth, S. Ott, *Dalton Trans.* **2009**, *45*, 9952 – 9959.
[8] a) L. Schwartz, G. Eilers, L. Eriksson, A. Gogoll, R. Lomoth, S. Ott, *Chem. Commun.* **2006**, 520 – 522; b) S. Ott, M. Kritikos, B. Åkermark, L. Sun, R. Lomoth, *Angew. Chem.* **2004**, *116*, 1024 – 1027; *Angew. Chem. Int. Ed.* **2004**, *43*, 1006 – 1009; c) F. Wang, M. Wang, X. Liu, K. Jin, W. Dong, G. Li, B. Åkermark, L. Sun, *Chem. Commun.* **2005**, 3221 – 3223.
[9] B. E. Barton, M. T. Olsen, T. B. Rauchfuss, *J. Am. Chem. Soc.* **2008**, *130*, 16834 – 16835.
[10] a) J. D. Lawrence, H. X. Li, T. B. Rauchfuss, *Chem. Commun.* **2001**, 1482 – 1483; b) J. D. Lawrence, H. X. Li, T. B. Rauchfuss, M. Bénard, M.-M. Rohmer, *Angew. Chem.* **2001**, *113*, 1818 – 1821; *Angew. Chem. Int. Ed.* **2001**, *40*, 1768 – 1771; c) S. Ott, M. Kritikos, B. Åkermark, L. Sun, *Angew. Chem.* **2003**, *115*, 3407 – 3410; *Angew. Chem. Int. Ed.* **2003**, *42*, 3285 – 3288.
[11] a) M. Razavet, S. C. Davies, D. L. Hughes, C. J. Pickett, *Chem. Commun.* **2001**, 847 – 848; b) S. J. George, Z. Cui, M. Razavet, C. J. Pickett, *Chem. Eur. J.* **2002**, *8*, 4037 – 4046; c) A. Silakov, J. L. Shaw, E. J. Reijerse, W. Lubitz, *J. Am. Chem. Soc.* **2010**, *132*, 17578 – 17587.
[12] F. Neese, *Coord. Chem. Rev.* **2009**, *253*, 526 – 563.
[13] Broken-symmetry DFT calculations with the BP86 and B3LYP functionals converged back to the delocalized $S = 1/2$ state and yielded identical results.
[14] M. L. Singleton, N. Bhuvanesh, J. H. Reibenspies, M. Y. Darensbourg, *Angew. Chem.* **2008**, *120*, 9634 – 9637; *Angew. Chem. Int. Ed.* **2008**, *47*, 9492 – 9495.
[15] a) A. Schweiger, G. Jeschke, *Principles of Pulsed Electron Paramagnetic Resonance*, Oxford University Press, New York, **2001**; b) W. Lubitz, E. Reijerse, M. van Gastel, *Chem. Rev.* **2007**, *107*, 4331 – 4365; c) S. A. Dikanov, Y. D. Tsvetkov, *Electron Spin Echo Envelope Modulation (ESEEM) Spectroscopy*, CRC, Boca Raton, FL, **1992**.
[16] a) The nuclear quadrupole coupling parameter, K, defined by $e^2 q Q/h = 4K$, contains the electric quadrupole moment eQ of the nucleus and the electric field gradient eq at the site of the nucleus. The asymmetry parameter $\eta = (P_x - P_y)/P_z$ gives the derivation from axial symmetry of the quadrupole tensor **P**, with convention $|P_z| > |P_y| \geq |P_x|$ and $0 \leq \eta \leq 1$. For details, see: b) E. A. C. Lucken, *Nuclear Quadrupole Coupling Constants*, Academic Press, London, **1969**.
[17] a) S. Sinnecker, F. Neese, *J. Comput. Chem.* **2006**, *27*, 1463 – 1475; b) J. N. Latosinska, *Int. J. Quantum Chem.* **2003**, *91*, 284 – 296; c) U. Ryde, C. Greco, L. De Gioia, *J. Am. Chem. Soc.* **2010**, *132*, 4512 – 4513.

